Computers and Structures 254 (2021) 106559

Contents lists available at ScienceDirect

Computers and Structures

journal homepage: www.elsevier.com/locate/compstruc

Selecting the load at the intermediate time point of the ρ_∞-Bathe time integration scheme

Sun-Beom Kwon [a], Klaus-Jürgen Bathe [b], Gunwoo Noh [c,*]

[a] Purdue University, West Lafayette, IN 47907, USA
[b] Massachusetts Institute of Technology, Cambridge, MA 02139, USA
[c] Korea University, Seoul 02841, Republic of Korea

ARTICLE INFO

Article history:
Received 15 February 2021
Accepted 7 April 2021

Keywords:
Direct time integrations
External loads
Implicit schemes
Bathe methods
Structural dynamics
Wave propagation

ABSTRACT

The objective of this paper is to identify the optimal load selection at the intermediate time point of the ρ_∞-Bathe time integration method. We study the truncation errors of the scheme in homogeneous and forced responses for various parameters. The optimal load at the sub-step is determined by minimizing the global truncation errors of forced responses. A numerical impulse analysis shows that the optimal load at the sub-step thus established actually corresponds to numerical impulses at the three- and four-point Newton-Cotes formulas for the second- and third-order accuracy cases, respectively. We illustrate the findings of our theoretical study in example solutions of two-dimensional structural dynamics and wave propagation problems. With the optimally selected load at the sub-step, more accurate solutions can be obtained in some analyses.

1. Introduction

In practical finite element analysis of structural dynamics and wave propagation problems, the dynamic equilibrium equations are frequently solved by direct time integration [1–3]. Then two types of schemes, explicit and implicit methods are used [3]. Since an explicit scheme is only conditionally stable, it may be effectively employed when the time step size required by the stability limit is comparable to the time step size needed by accuracy considerations, i.e., in impact, crash, and short time wave propagations. On the other hand, an implicit scheme can be unconditionally stable, and such scheme is often preferred.

Many implicit time integration schemes have been proposed, and much effort has been devoted to finding the best use [4–12]. In the last decade, in particular, much research effort has been focused on developing new time integrations based on the composite strategy with sub-steps [13–25] after the introduction of its first kind, the standard Bathe method [26–27]. Recently, as a generalization of the standard and β_1/β_2-Bathe schemes [28–29], the ρ_∞-Bathe method was proposed by Noh and Bathe [30]. The spectral properties of the method can be changed effectively with one-parameter, ρ_∞. The ρ_∞-Bathe method contains as special cases the standard and β_1/β_2-Bathe schemes and the Newmark method at its best use [31]. Recently, the effective use of the Bathe schemes in wave propagation analysis with linear finite elements was studied [32].

The Bathe methods split the time step into two sub-steps. The methods can be first, second or third-order accurate, depending on the values of the parameters, but these assessments were all carried out – as is usual – looking only at the non-forced response solution, that is, considering only initial conditions, see Refs. [28–34]. In practice of course, loading is applied and hence we need to understand the behavior of a time integration method when loading is used.

Using the Bathe methods, it is important to see that all calculations in the sub-step may be regarded as part of an "internal procedure" per step.

Namely, the key point is that the solution at the intermediate time point is only used for the calculation of the solution at the full step [26–34]. Any reasonable procedure in the sub-step calculation is a candidate to improve the complete solution scheme.

It therefore follows from the underlying principle of the basic strategy, that we may modify the procedure or values of parameters used in the calculations of the sub-step. Of course, it then needs to be demonstrated that the novel procedure is effective. In this paper, we focus on the different use of the externally applied load in the equilibrium equations at the intermediate time point.

* Corresponding author.
E-mail address: gunwoonoh@korea.ac.kr (G. Noh).

https://doi.org/10.1016/j.compstruc.2021.106559
0045-7949/

For single-step methods, only some research efforts have been directed to the modification of the external loads for the cases of rapidly varying or impulsive loads. For the use of a larger time step in the solution of problems with rapidly varied loads, the momentum equations of motions were used instead of force equilibrium [35–37]. Other strategies to overcome the difficulty arising from the load discontinuity are the use of a single small time step, when needed, near the change of the load intensity [38], or adjusting the input load at the instant of load discontinuity [39]. For adjusting the input load, the assumed load at the load discontinuity is set to the average of the two discontinuity values for the trapezoidal rule. In the Noh-Bathe explicit method [41], when the external loads are only available at the full step, the load is established according to a numerical impulse analysis at the intermediate time point; otherwise, the given load is used.

Our objective in the present study is to understand the effect of the magnitude of the load value at the sub-step on the solution accuracy of the ρ_∞-Bathe scheme. This then enables us to identify the optimal load value to be used at the sub-step, based on mimimizing the numerical errors. In particular, we may want to choose the load value such that the possible order of accuracy (with no external load applied) is not reduced. We use two approaches to select appropriate loads at the sub-step for the ρ_∞-Bathe schemes: a truncation error analysis [43] and a numerical impulse analysis [41]. Using the truncation error approach, we determine the optimal selection of the load at the sub-step by minimizing the global truncation error of the forced response solution. Thereafter, using the numerical impulse approach we study how an impulse at the sub-step affects the response and can identify based on this approach also the optimal load at the sub-step. The results from both approaches are shown to be identical.

In Section 2, we study the local and global truncation errors for the ρ_∞-Bathe method using various values of parameters. In Section 3, a load selection strategy based on the numerical impulse analysis is presented. In Section 4, we provide numerical results obtained using various sub-step loads in the solutions of a single-degree-of-freedom problem, a 2D structural dynamics problem, and a 2D wave propagation problem. These solutions illustrate the findings of our theoretical study.

2. Truncation error analysis

In this section, we first establish truncation errors in homogeneous and forced responses. We then seek the solution errors of the ρ_∞-Bathe method on both a local and global scale with its two-level form. The *local truncation error* is the truncation error that occurs in one step of the time integration scheme. The *global truncation error* is the truncation error that accumulates in the solution of a problem over the complete time domain considered.

Once we have established the global truncation error, we can identify the optimal load to be used at the sub-step. This load minimizes the global truncation error of the particular solution (forced response).

In the following we use a simplified notation, for example the time step is now $h = \Delta t$ (Δt was used earlier [3]). This enables us to focus more easily on the essence of the analysis.

2.1. Energy-based error measure

The equations of motion in linear structural dynamics are, see e.g. Ref. [3],

$$\begin{pmatrix} \dot{\boldsymbol{u}} \\ \dot{\boldsymbol{v}} \end{pmatrix} = \begin{pmatrix} \boldsymbol{0} & \boldsymbol{I} \\ -\boldsymbol{M}^{-1}\boldsymbol{K} & -\boldsymbol{M}^{-1}\boldsymbol{C} \end{pmatrix} \begin{pmatrix} \boldsymbol{u} \\ \boldsymbol{v} \end{pmatrix} + \begin{pmatrix} \boldsymbol{0} \\ \boldsymbol{M}^{-1}\boldsymbol{f} \end{pmatrix} \tag{1}$$

or

$$\dot{\boldsymbol{x}} = \boldsymbol{F}\boldsymbol{x} + \boldsymbol{g} \tag{2}$$

with the analytical solution for the response at time t

$$\tilde{\boldsymbol{x}}(t) = e^{\boldsymbol{F}(t-t_0)}\boldsymbol{x}(t_0) + \int_{t_0}^{t} e^{\boldsymbol{F}(t-\tau)}\boldsymbol{g}(\tau)d\tau \tag{3}$$

where $\boldsymbol{M}$, $\boldsymbol{C}$, $\boldsymbol{K}$, $\boldsymbol{f}$, $\boldsymbol{v}$, and $\boldsymbol{u}$ are the mass, damping, stiffness matrices, external forces (moments), velocity, and displacement vectors, respectively, and an overdot denotes a time derivative.

The first and second terms of the right-hand side of Eq. (3) represent the homogeneous and particular solutions, respectively.

We define the energy-based error measure as

$$E(t) := \frac{1}{\sqrt{2}} \| \boldsymbol{\Gamma}^{1/2}\boldsymbol{E}_{\boldsymbol{x}}(t) \|_2 \tag{4}$$

where $\boldsymbol{\Gamma} := \mathrm{diag}(\boldsymbol{K}, \boldsymbol{M})$ is the block diagonal scaling matrix and $\boldsymbol{E}_{\boldsymbol{x}}(t)$ is the error vector of the displacement and velocity $\boldsymbol{E}_{\boldsymbol{x}}(t) = \left[\boldsymbol{u}(t) - \tilde{\boldsymbol{u}}(t);\ \boldsymbol{v}(t) - \tilde{\boldsymbol{v}}(t)\right]$. Here, $\tilde{\boldsymbol{u}}(t)$ and $\tilde{\boldsymbol{v}}(t)$ are the analytical solutions obtained using Eq. (3).

2.2. Calculation of errors with a two-level formulation

The ρ_∞-Bathe method uses the trapezoidal rule in its first sub-step with time step size γh, where γ is the time step splitting ratio. In linear dynamic analysis, we use with the equilibrium equations at the end of the sub-step [3]:

$$\boldsymbol{M}\boldsymbol{a}_{n+\gamma} + \boldsymbol{C}\boldsymbol{v}_{n+\gamma} + \boldsymbol{K}\boldsymbol{u}_{n+\gamma} = \hat{\boldsymbol{f}}_{n+\gamma} \tag{5}$$

$$\boldsymbol{u}_{n+\gamma} = \boldsymbol{u}_n + \frac{\gamma h}{2}\left[\boldsymbol{v}_n + \boldsymbol{v}_{n+\gamma}\right] \tag{6}$$

$$\boldsymbol{v}_{n+\gamma} = \boldsymbol{v}_n + \frac{\gamma h}{2}\left[\boldsymbol{a}_n + \boldsymbol{a}_{n+\gamma}\right] \tag{7}$$

where $\boldsymbol{a}$ denotes an acceleration vector. Here the externally applied load $\hat{\boldsymbol{f}}_{n+\gamma}$ is the load actually used for the sub-step calculation and may not be the same as the given external force at time $(n+\gamma)h$, $\boldsymbol{f}_{n+\gamma}$.

Note that in Eqs. (5)–(7) we introduce another simplification of the notation; namely in all subscripts for the solution and external force vectors we denote the time $nh = n\Delta t = t$ and γh simply as n and γ, respectively, but this notation is only used for subscripts.

In the second sub-step, the following relations are used with the parameters q_0, q_1, q_2, s_0, s_1, and s_2 for the equilibrium at the end of the full step, from n to $n+1$:

$$\boldsymbol{M}\boldsymbol{a}_{n+1} + \boldsymbol{C}\boldsymbol{v}_{n+1} + \boldsymbol{K}\boldsymbol{u}_{n+1} = \boldsymbol{f}_{n+1} \tag{8}$$

$$\boldsymbol{u}_{n+1} = \boldsymbol{u}_n + h\left[q_0\boldsymbol{v}_n + q_1\boldsymbol{v}_{n+\gamma} + q_2\boldsymbol{v}_{n+1}\right] \tag{9}$$

$$\boldsymbol{v}_{n+1} = \boldsymbol{v}_n + h\left[s_0\boldsymbol{a}_n + s_1\boldsymbol{a}_{n+\gamma} + s_2\boldsymbol{a}_{n+1}\right] \tag{10}$$

The ρ_∞-Bathe scheme has second-order accuracy with and without damping when the following relations are used

$$q_1 = s_1 = \frac{\rho_\infty + 1}{2\gamma(\rho_\infty - 1) + 4};\ q_0 = s_0 = (\gamma - 1)q_1 + \frac{1}{2};\ \text{and}$$
$$q_2 = s_2 = -\gamma q_1 + \frac{1}{2} \tag{11}$$

With a proper set of values of the parameters, the ρ_∞-Bathe scheme reduces to the standard-Bathe, β_1/β_2-Bathe, and the (two-step) Newmark method with $\alpha = 0.25(\delta + 0.5)^2$. Hence the ρ_∞-Bathe method "contains" these schemes as special cases [31].

In Ref. [31], we also give the condition for third-order accuracy in the period elongation and amplitude decay using the ρ_∞-Bathe

method with $\rho_\infty \in (-1, 1-\sqrt{3}]$. We refer to Ref. [44] for the details of the higher-order ρ_∞-Bathe scheme with a larger range of ρ_∞ including $\rho_\infty \in [0,1]$ in the solution of structural dynamics and heat flow problems.

With the equilibrium equations at time nh, $(n+\gamma)h$, and $(n+1)h$, the ρ_∞-Bathe scheme can be rewritten into the form

$$\begin{pmatrix} \frac{\gamma h}{2}\boldsymbol{K} & \boldsymbol{M}+\frac{\gamma h}{2}\boldsymbol{C} \\ \boldsymbol{I} & -\frac{\gamma h}{2}\boldsymbol{I} \end{pmatrix}\begin{pmatrix} \boldsymbol{u}_{n+\gamma} \\ \boldsymbol{v}_{n+\gamma} \end{pmatrix} = \begin{pmatrix} -\frac{\gamma h}{2}\boldsymbol{K} & \boldsymbol{M}-\frac{\gamma h}{2}\boldsymbol{C} \\ \boldsymbol{I} & \frac{\gamma h}{2}\boldsymbol{I} \end{pmatrix}\begin{pmatrix} \boldsymbol{u}_{n} \\ \boldsymbol{v}_{n} \end{pmatrix} + \begin{pmatrix} \frac{\gamma h}{2}\left(\boldsymbol{f}_n + \hat{\boldsymbol{f}}_{n+\gamma}\right) \\ \boldsymbol{0} \end{pmatrix} \tag{12}$$

$$\begin{pmatrix} hs_2\boldsymbol{K} & \boldsymbol{M}+hs_2\boldsymbol{C} \\ \boldsymbol{I} & -hq_2\boldsymbol{I} \end{pmatrix}\begin{pmatrix} \boldsymbol{u}_{n+1} \\ \boldsymbol{v}_{n+1} \end{pmatrix} = \begin{pmatrix} -hs_1\boldsymbol{K} & -hs_1\boldsymbol{C} \\ \boldsymbol{I} & hq_1\boldsymbol{I} \end{pmatrix}\begin{pmatrix} \boldsymbol{u}_{n+\gamma} \\ \boldsymbol{v}_{n+\gamma} \end{pmatrix} + \begin{pmatrix} -hs_0\boldsymbol{K} & \boldsymbol{M}-hs_0\boldsymbol{C} \\ \boldsymbol{I} & hq_0\boldsymbol{I} \end{pmatrix}\begin{pmatrix} \boldsymbol{u}_{n} \\ \boldsymbol{v}_{n} \end{pmatrix} + \begin{pmatrix} h\left(s_0\boldsymbol{f}_n + s_1\hat{\boldsymbol{f}}_{n+\gamma} + s_2\boldsymbol{f}_{n+1}\right) \\ \boldsymbol{0} \end{pmatrix} \tag{13}$$

Substituting Eq. (12) into Eq. (13), we obtain the following two-level form for a typical modal equation of Eq. (1), $a + 2\xi\omega_0 v + \omega_0^2 u = f$ with damping ratio ξ, natural frequency ω_0 and external force f,

$$\boldsymbol{x}_n = \boldsymbol{A}^n\boldsymbol{x}_0 + \boldsymbol{B}_n \tag{14}$$

where $\boldsymbol{x}$, $\boldsymbol{A}$ and $\mathbf{B}$ are the state vector, amplification matrix, and load vector related to the forced response, respectively (See Appendix), with n (n = 1,2,3, ..) denoting here the state to be calculated and we have

$$\boldsymbol{x}_n = \begin{bmatrix} u_n & v_n \end{bmatrix}^T; \quad \boldsymbol{B}_n = \sum_{k=0}^{n-1}\boldsymbol{A}^{n-k-1}\boldsymbol{b}_k \tag{15}$$

where $\boldsymbol{b}_n$ is the direct load vector at time nh. Here u_n and v_n are the displacement and velocity at time t.

We can now establish the energy-based error in Eq. (4). Considering the time domain 0 to nh with $\boldsymbol{x}_0 = \tilde{\boldsymbol{x}}(0)$, we obtain the following relation:

$$\begin{aligned} E(nh) &:= \frac{1}{\sqrt{2}}\parallel \boldsymbol{\Gamma}^{1/2}\left((\boldsymbol{A}^n - e^{\boldsymbol{F}nh})\boldsymbol{x}_0 + \boldsymbol{B}_n - \int_0^{nh} e^{\boldsymbol{F}(nh-\tau)}g(\tau)d\tau\right)\parallel_2 \\ &\leqslant \frac{1}{\sqrt{2}}\parallel \boldsymbol{\Gamma}^{1/2}\left((\boldsymbol{A}^n - e^{\boldsymbol{F}nh})\boldsymbol{x}_0\right)\parallel_2 \\ &\quad + \frac{1}{\sqrt{2}}\parallel \boldsymbol{\Gamma}^{1/2}\left(\boldsymbol{B}_n - \int_0^{nh} e^{\boldsymbol{F}(nh-\tau)}g(\tau)d\tau\right)\parallel_2 \end{aligned} \tag{16}$$

Note that the first component in Eq. (16) captures error in the initial energy $E_0 := \parallel \boldsymbol{\Gamma}^{1/2}\boldsymbol{x}_0 \parallel_2^2/2$. With the assumption of positive definiteness of $\boldsymbol{\Gamma}$ (that is, the stiffness matrix $\boldsymbol{K}$and $\boldsymbol{M}$ are positive definite), this dependency is removed by maximization over all initial conditions with unit energy [43]. Therefore, we define the errors related to the homogeneous and forced responses as $E_1(nh)$ and $E_2(nh)$, respectively:

$$\begin{aligned} E_1(nh) &:= \parallel \boldsymbol{\Gamma}^{1/2}\left((\boldsymbol{A}^n - e^{\boldsymbol{F}nh})\boldsymbol{x}_0\right)\boldsymbol{\Gamma}^{-1/2}\parallel_2 \\ E_2(nh) &:= \tfrac{1}{\sqrt{2}}\parallel \boldsymbol{\Gamma}^{1/2}\left(\boldsymbol{B}_n - \int_0^{nh} e^{\boldsymbol{F}(nh-\tau)}g(\tau)d\tau\right)\parallel_2 \end{aligned} \tag{17}$$

where $E_2(nh)$ depends on the external loads.

Considering the leading-order terms of the Taylor series expansion of these error expressions around $h = 0$, we show below that the orders of accuracy of the time integration scheme are given by

$$E_1(nh) \approx C_1^l h^{k_1+1}, \quad E_2(nh) \approx C_2^l h^{k_2+1} \tag{18}$$

where we consider the local truncation errors, k_1 and k_2 are the orders of solution accuracy, and C_1^l and C_2^l are constants calculated from the limiting behavior of $E_1(nh)$ and $E_2(nh)$, respectively, when the time step size approaches zero. We shall see that, as expected, the global truncation errors are of one order lower than the local errors.

2.3. Local errors in the calculations of homogeneous and forced responses

We first discuss the case of 2nd order accuracy in the solution and then proceed to the case of third order solution accuracy.

Case of 2nd order accuracy in the solution

The Taylor series expansion of $E_1(nh)$ in Eq. (17) for the ρ_∞-Bathe scheme gives

$$\begin{aligned} E_1(nh) &= \frac{\sigma_1\omega_0^2 nh^3}{6}\sqrt{\eta_1 + \sqrt{\eta_1^2 - \eta_2^2}} + O^l\left(h^4\right) \\ \eta_1 &= 2\omega_0^2\xi^2 + \left(\omega_0^4 + 1\right)\left(1 - 4\xi^2\right)^2/2 + 8\omega_0^6\xi^2\left(1 - 2\xi^2\right)^2 \\ \eta_2 &= \omega_0^2\left(1 - 4\xi^2\right)^2 - 8\omega_0^4\xi^2\left(1 - 2\xi^2\right) \\ \sigma_1 &= \tfrac{3\gamma(\gamma-1)(\rho_\infty+1)}{2\gamma(\rho_\infty-1)+4} + \tfrac{1}{2} \end{aligned} \tag{19}$$

with the superscript l in O^l signifying "local". Since the exponent on h in Eq. (19) is "3", this error corresponds to second order accuracy in the overall solution (see Section 2.4).

To analyze the solution corresponding to the forced response, we consider a periodic load since a general load can frequently be expressed as a Fourier sum of harmonic functions. We focus on the error when a sinusoidal load$f(t) = \sin\omega t$, $\omega \neq \omega_0$ is applied to find an effective load value at the intermediate time point.

To establish the load at the sub-step with the given external load data, we use the following relation:

$$\hat{f}_{n+\gamma} = w_{-1}f_{n-1} + w_{-1+\gamma}f_{n-1+\gamma} + w_0 f_n + w_\gamma f_{n+\gamma} + w_1 f_{n+1} \tag{20}$$

where w_{-1}, $w_{-1+\gamma}$, w_0, w_γ, and w_1 are "weights on the loading" corresponding to the directly evaluated loads f_{n-1}, $f_{n-1+\gamma}$, f_n, $f_{n+\gamma}$, and f_{n+1}. Hence $f_{n+\gamma}$ is the given external load value at time $(n+\gamma)\Delta t$, and $\hat{f}_{n+\gamma}$ is the selected load used in the calculation of the first sub-step to obtain, if possible, a more accurate response solution.

Using the Taylor series expansion around f_n, we obtain the first condition for the weights that should be satisfied

$$w_{-1} + w_{-1+\gamma} + w_0 + w_\gamma + w_1 = 1 \tag{21}$$

and for a sinusoidal loading, we obtain from the Maclaurin series expansion of $\int_0^{nh} e^{(\boldsymbol{F}(nh-\tau))}\sin(\omega\tau)d\tau$ (See, Eq. (3))

$$\int_0^{nh} e^{\boldsymbol{F}(nh-\tau)}\sin(\omega\tau)d\tau = \begin{bmatrix} \frac{\omega n^3h^3}{6} - \frac{\xi\omega_0\omega n^4h^4}{12} + O^l\left(h^5\right) \\ \frac{\omega n^2h^2}{2} - \frac{\xi\omega_0\omega n^3h^3}{3} - \frac{\omega n^4h^4}{24}\left(\omega^2 + \omega_0^2(1-4\xi^2)\right) + O^l\left(h^5\right) \end{bmatrix} \tag{22}$$

where the first and second rows correspond to the displacement and velocity components, respectively.

The difference between the numerical and analytical load vectors in one timestep is hence

$$\boldsymbol{B}_0 - \int_0^h e^{\boldsymbol{F}(h-\tau)}\sin(\omega\tau)d\tau = \begin{bmatrix} O^l\left(h^3\right) \\ \left(w_1 + w_\gamma\gamma + w_{-1+\gamma}(\gamma-1) - w_{-1} - \gamma\right)\omega h^2 + O^l\left(h^3\right) \end{bmatrix} \tag{23}$$

Therefore, in order to have second-order accuracy in the solution for the forced response we use

$$w_1 = \gamma\left(1 - w_\gamma\right) + w_{-1+\gamma}(1-\gamma) + w_{-1} \tag{24}$$

With Eqs. (21) and (24), the error on the forced response becomes

$$E_2(nh) = \frac{\sigma_1 \omega n h^3}{6\sqrt{2}} \sqrt{1 + \xi^2 \omega_0^4} + O^l\left(h^4\right) \tag{25}$$

From the derivatives of $E_1(nh)$ in Eq. (19) and $E_2(nh)$ in Eq. (25) with respect to γ, we obtain the expression of γ in terms of $\rho_\infty \in [0,\ 1]$ to have the minimum errors for both the homogeneous and forced responses of the second-order accurate ρ_∞-Bathe method as

$$\gamma_0 = \frac{2 - \sqrt{2 + 2\rho_\infty}}{1 - \rho_\infty}; \quad \gamma_0 = 0.5 \text{ if } \rho_\infty = 1 \tag{26}$$

We note that this value of γ is also the value to use to have identical effective stiffness matrices for each sub-step, and the maximum (locally) amplitude decay and minimum (globally) period elongation, as reported in Ref. [30].

Case of 3rd order accuracy in the solution

Since Eqs. (19) and (25) are general expressions, they also provide ρ_∞ in terms of γ to have third-order accuracy in the solution for both the homogeneous and forced responses. Using $\sigma_1 = 0$ in Eq. (19) leads to

$$\begin{gathered} E_1(nh) = \frac{\sigma_2 \omega_0^3 n h^4}{24} \sqrt{\tilde{\eta}_1 + \sqrt{\tilde{\eta}_1^2 - \tilde{\eta}_2^2}} + O^l\left(h^5\right) \\ \tilde{\eta}_1 = \omega_0^2 \left(1 - 4\xi^2\right)^2 / 2 + 8\left(\omega_0^4 + 1\right)\xi^2 \left(1 - 2\xi^2\right)^2 + \omega_0^6 \left(16\xi^4 - 12\xi^2 + 1\right)^2 / 2 \\ \tilde{\eta}_2 = 16\omega_0^2 \xi^2 \left(1 - 2\xi^2\right)^2 + \omega_0^4 \left(1 - 4\xi^2\right)\left(16\xi^4 - 12\xi^2 + 1\right) \\ \sigma_2 = \frac{\gamma(3\gamma^2 - 2)(\rho_\infty + 1)}{\gamma(\rho_\infty - 1) + 2} + 1 \end{gathered} \tag{27}$$

which corresponds to third order accuracy in the solution of the homogeneous response. Using $\sigma_1 = 0$ as well in Eq. (25) gives also third-order accuracy in the forced response solution.

Then minimizing the error in both the homogeneous and forced responses of the third-order accurate ρ_∞-Bathe method with respect to γ gives then

$$\gamma_p = \frac{\rho_\infty + 2 - \sqrt{\rho_\infty^2 - 2\rho_\infty - 2}}{3(\rho_\infty + 1)}; \quad \rho_\infty \in (-1,\ 1 - \sqrt{3}] \tag{28}$$

for which indeed σ_1 in Eq. (19) equals 0. Note that the relation in Eq. (28) is identical to the condition for the ρ_∞-Bathe method to have third-order accuracy as derived from the period elongation and amplitude decay, see Ref. [31].

Using Eq. (28), that is, considering the ρ_∞-Bathe method with third-order accuracy, the leading term in the error of the forced response solution is of order of 4, and is a function of the weights on the loading

$$\begin{gathered} E_2(nh) = \frac{\omega_0 \omega n h^4}{12\sqrt{2}} \sqrt{\left(\omega^2(3n\alpha + q_1\beta) + \omega_0^2\left(1 - 4\xi^2\right)\sigma_2\right)^2 + 2\xi^2\sigma_2^2} + O^l\left(h^5\right) \\ \alpha = w_\gamma \gamma q_1(\gamma - 1) + w_{-1+\gamma} q_1(\gamma - 1)(\gamma - 2) + 2w_{-1} q_1 + 1/6 \\ \beta = w_\gamma \gamma(2\gamma - 1)(\gamma - 1) + w_{-1+\gamma}(\gamma - 1)\left(2\gamma^2 - 7\gamma + 6\right) - 6w_{-1} \end{gathered} \tag{29}$$

Hence, in this case, both local errors $E_1(nh)$ and $E_2(nh)$ are proportional to h^4.

2.4. Global errors in the calculations of the homogeneous and forced responses

When $n = T/h$ (here, T is the considered time duration), we can calculate the global truncation errors based on the local truncation errors to be

$$E_1(T) \approx C_1^g h^{k_1}, E_2(T) \approx C_2^g h^{k_2} \tag{30}$$

where C_1^g and C_2^g are constants for $E_1(T)$ and $E_2(T)$, respectively.

Substituting $n = T/h$ into Eqs. (19) and (25), the global truncation errors of the second-order accurate ρ_∞-Bathe scheme are

$$E_1(T) = \frac{\sigma_1 \omega_0^2 T h^2}{6} \sqrt{\eta_1 + \sqrt{\eta_1^2 - \eta_2^2}} + O^g\left(h^3\right) \tag{31}$$

$$E_2(T) = \frac{\sigma_1 \omega T h^2}{6\sqrt{2}} \sqrt{1 + 4\xi^2 \omega_0^4} + O^g\left(h^3\right) \tag{32}$$

We may actually reduce the error by minimizing $E_2(T)$ with appropriate weights on the loading. For the weights to be independent of ω_0, ω, and ξ, the condition for the summation of the terms related to the weights to be zero leads to the following relation:

$$\begin{aligned} w_\gamma = {} & \frac{1}{2\gamma q_1} \frac{n}{(1 - \gamma)(2\gamma + (3n - 1))} + \frac{2\gamma^2 + (3n - 7)\gamma - 6(n - 1)}{-\gamma(2\gamma + (3n - 1))} w_{-1+\gamma} \\ & + \frac{6(n - 1)}{\gamma(1 - \gamma)(2\gamma + (3n - 1))} w_{-1} \end{aligned} \tag{33}$$

When $n \to \infty$, Eq. (33) gives

$$\lim_{n \to \infty} w_\gamma = \frac{1}{6\gamma q_1 (1 - \gamma)} + \frac{2 - \gamma}{\gamma} w_{-1+\gamma} + \frac{2}{\gamma(1 - \gamma)} w_{-1} \tag{34}$$

Therefore, for the second-order accurate ρ_∞-Bathe method with γ_0 the error in the forced response is minimized when the load at the intermediate time point is selected using the weights satisfying Eqs. (21), (24) and (34).

For the third-order accurate ρ_∞-Bathe method, we obtain the global truncation errors from Eqs. (27) and (29):

$$E_1(T) = \frac{\sigma_2 \omega_0^3 T h^3}{24} \sqrt{\tilde{\eta}_1 + \sqrt{\tilde{\eta}_1^2 - \tilde{\eta}_2^2}} + O^g\left(h^4\right) \tag{35}$$

$$\begin{aligned} E_2(T) = {} & \frac{\omega_0 \omega T h^3}{12\sqrt{2}} \sqrt{\left(3\alpha\omega^2 T/h + q_1\beta\omega^2 + \left(1 - 4\xi^2\right)\sigma_2\omega_0^2\right)^2 + 2\xi^2\sigma_2^2} \\ & + O^g\left(h^4\right) \end{aligned} \tag{36}$$

To minimize the error in the forced response, we use Eq. (34) and the relation obtained by forcing the term related to ω in $O^g\left(h^3\right)$ of Eq. (36) to become zero:

$$w_{-1+\gamma} = \frac{\gamma(1 - 2\gamma)}{(2\gamma^2 - 7\gamma + 6)} w_\gamma + \frac{6}{(\gamma - 1)(2\gamma^2 - 7\gamma + 6)} w_{-1} \tag{37}$$

Hence we use with γ_p given in Eq. (34) also Eq. (37) to minimize the amount of the error. Therefore, for the third-order accurate ρ_∞-Bathe method with γ_p, the weights on the loading may be determined using Eqs. (21), (24), (34) and (37).

2.5. The loading for minimum global errors in the forced response calculations

For the second-order accurate ρ_∞-Bathe method, the equations related to the weights on the loading are Eqs. (21), (24), and (34). Therefore we can determine the optimal loading using just three time points:

$$\hat{f}_{n+\gamma} = w_0 f_n + w_\gamma f_{n+\gamma} + w_1 f_{n+1} \tag{38}$$

where we set $w_{-1} = w_{-1+\gamma} = 0$. The optimal loading at the substep becomes

$$\hat{f}_{n+\gamma} = \frac{6\gamma q_1(1-\gamma)-1}{6\gamma q_1} f_n + \frac{1}{6\gamma q_1(1-\gamma)} f_{n+\gamma} + \frac{6\gamma q_1(1-\gamma)-1}{6q_1(1-\gamma)} f_{n+1} \tag{39}$$

Using Eq. (39) with the second-order accurate ρ_∞-Bathe method, provides more accurate solutions than the use of the given load. However, we note that using the load in Eq. (39) for the third order accurate method, i.e. using Eq. (28), simply gives $\hat{f}_{n+\gamma} = f_{n+\gamma}$.

For the third-order accurate ρ_∞-Bathe method, the equations related to the weights on the loading are instead Eqs. (21), (24), (34), and (37). Therefore, we use four time points, which leads to

$$\begin{aligned}\hat{f}_{n+\gamma} &= w_{\gamma-1} f_{n-1+\gamma} + w_0 f_n + w_\gamma f_{n+\gamma} + w_1 f_{n+1} \\ &= \frac{1-2\gamma}{12q_1(1-\gamma)(2-\gamma)} f_{n-1+\gamma} + \left(1-\gamma-\frac{4\gamma^2-11\gamma+6}{12\gamma q_1(1-\gamma)(2-\gamma)}\right) f_n \\ &\quad + \frac{2\gamma^2-7\gamma+6}{12\gamma q_1(1-\gamma)(2-\gamma)} f_{n+\gamma} + \left(\gamma + \frac{4\gamma-5}{12q_1(1-\gamma)(2-\gamma)}\right) f_{n+1}\end{aligned} \tag{40}$$

We note that the loads selected at the sub-step from Eqs. (39) and (40) are identical to the loads obtained from the three-point and four-point Newton-Cotes formulas [3], respectively (see Section 3.2).

3. Numerical impulse analysis

A typical modal equation of Eq. (1) is

$$a + 2\xi\omega_0 v + \omega_0^2 u = f \tag{41}$$

where ξ, ω_0, and f are damping ratio, natural frequency and external force, respectively.

Integrating Eq. (41) from t to $t+h$, we obtain

$$\int_t^{t+h} (f - \omega_0^2 u)dt = \int_t^{t+h} (a + 2\xi\omega_0 v)dt \tag{42}$$

or

$$\int_t^{t+h} (f - \omega_0^2 u)dt = \int_t^{t+h} dv + 2\xi\omega_0 \int_t^{t+h} du \tag{43}$$

Using the ρ_∞-Bathe scheme (Eqs. (9) and (10)) for Eq. (43), we obtain

$$\int_t^{t+h} (f - \omega_0^2 u)dt = h\left[q_0 f_n + q_1 \hat{f}_{n+\gamma} + q_2 f_{n+1} - \omega_0^2 (q_0 u_n + q_1 u_{n+\gamma} + q_2 u_{n+1})\right] \tag{44}$$

Since Eq. (44) holds for the general loading and trajectory, we have

$$\int_t^{t+h} f dt\Big|_{\rho_\infty\text{ - Bathe}} = h\left(q_0 f_n + q_1 \hat{f}_{n+\gamma} + q_2 f_{n+1}\right) \tag{45}$$

3.1. Sub-step load from the two-point closed Newton-Cotes quadrature rule

In many practical problems, external loads are only given at discrete time points. If the external forces are only given at times t and $t+h$ as f_n and f_{n+1}, we may use

$$\int_t^{t+h} f dt = h[\alpha f_n + (1-\alpha) f_{n+1}] \tag{46}$$

where α is a weight.

Using Eqs. (45) and (46), we obtain the load at the sub-step for the ρ_∞-Bathe scheme to be

$$\hat{f}_{n+\gamma} = (1-\gamma) f_n + \gamma f_{n+1} + \frac{(\alpha - 0.5)}{q_1}(f_n - f_{n+1}) \tag{47}$$

In general, the case $\alpha = 0.5$ yields the most accurate approximation; thus we use $\alpha = 0.5$ to approximate the numerical impulse when external loads are defined only at discrete time points, h apart. In this case, the external force at the sub-step is selected as

$$\hat{f}_{n+\gamma} = (1-\gamma) f_n + \gamma f_{n+1} \tag{48}$$

This means we have $(w_{-1}, w_{-1+\gamma}, w_0, w_\gamma, w_1) = (0, 0, 1-\gamma, 0, \gamma)$ in Eq. (20), which satisfies Eqs. (21) and (24), but not Eq. (34). Therefore, the selected load at the sub-step by Eq. (48) provides second-order accuracy in forced response; however, the error is larger than when the load in Eq. (39) or a given load, $f_{n+\gamma}$, is used. Therefore, the load obtained from the trapezoidal rule in Eq. (48) is recommended only when the load data is not available at the intermediate time point [45].

3.2. Sub-step loads from the three-, four-, and five-point Newton-Cotes formulas

For the case that external loads at the intermediate time points are available, we can use the three-point Newton-Cotes formula to approximate the numerical impulse by considering the time points t, $t+\gamma h$, and $t+h$:

$$\int_t^{t+h} f dt\Big|_{\text{3 - point}} = \frac{h/6}{\gamma(1-\gamma)}\left[(1-\gamma)(3\gamma-1) f_n + f_{n+\gamma} + \gamma(2-3\gamma) f_{n+1}\right] \tag{49}$$

With Eqs. (45) and (49), we obtain the load at the sub-step which renders the numerical impulse of the ρ_∞-Bathe scheme to be identical to the impulse obtained by the three-point Newton-Cotes formula:

$$\hat{f}_{n+\gamma} = \frac{\gamma(\rho_\infty - 1) + 2}{3\gamma(1-\gamma)(\rho_\infty + 1)} f_{n+\gamma} + \frac{(2-3\gamma)\gamma\rho_\infty - 3\gamma^2 + 4\gamma - 2}{3(\rho_\infty + 1)}\left(\frac{f_n}{\gamma} + \frac{f_{n+1}}{(1-\gamma)}\right) \tag{50}$$

We note that Eq. (50) is identical to Eq. (39).

Also, we may approximate the numerical impulse with the four-point Newton-Cotes formula by using the external loads at time $t + (\gamma - 1)h$, t, $t+\gamma h$, and $t+h$:

$$\int_t^{t+h} f dt\Big|_{\text{4 - point}} = \frac{h/12}{\gamma(1-\gamma)(2-\gamma)} \times \begin{bmatrix} \gamma(1-2\gamma) f_{n-1+\gamma} + (\gamma-2)(6\gamma^2 - 10\gamma + 3) f_n \\ + (2\gamma^2 - 7\gamma + 6) f_{n+\gamma} + \gamma(6\gamma^2 - 14\gamma + 7) f_{n+1} \end{bmatrix} \tag{51}$$

and, with Eqs. (45) and (51), the corresponding load at the sub-step becomes

$$\begin{aligned}\hat{f}_{n+\gamma} &= \frac{(1-2\gamma)(\gamma\rho_\infty - \gamma + 2)}{6(1-\gamma)(2-\gamma)(\rho_\infty + 1)} f_{n-1+\gamma} + \left(\frac{(4\gamma-3)}{3\gamma(\rho_\infty+1)} + \frac{6\gamma^2 - 8\gamma + 3}{6(1-\gamma)}\right) f_n \\ &\quad + \left(\frac{3-2\gamma}{6(1-\gamma)} + \frac{3-2\gamma}{3\gamma(\rho_\infty+1)}\right) f_{n+\gamma} + \left(\frac{\gamma(6\gamma^2 - 14\gamma + 7)}{6(1-\gamma)(2-\gamma)} + \frac{4\gamma-5}{3(2-\gamma)(\rho_\infty+1)}\right) f_{n+1}\end{aligned} \tag{52}$$

Notably, Eq. (52) is identical to the result from the global truncation error analysis for the third-order accurate ρ_∞-Bathe scheme, Eq. (40).

Table 1
Selection of the load at the intermediate time point of the ρ_∞-Bathe method.

(1) For second-order accurate method in displacement, velocity and acceleration (with $\gamma = \gamma_0$ in Eq. (26) and $\rho_\infty \in [0,\ 1]$):
Use the load selected by three-point Newton-Cotes rule, $\hat{f}_{n+\gamma}$ in Eq. (39) (=Eq.(50)) which minimizes the global errors in forced responses, with mimimum number of load data.
(2) For third-order accurate method in displacement, velocity and acceleration (with $\gamma = \gamma_p$ in Eq. (28) and $\rho_\infty \in (-1,\ 1-\sqrt{3}]$):
Use the load selected by four-point Newton-Cotes rule, $\hat{f}_{n+\gamma}$ in Eq. (40) (=Eq.(52)) which minimizes the global errors in forced responses, with mimimum number of load data.
(3) When the load data is not available at the intermediate time point:
Use the load selected by trapezoidal rule, $\hat{f}_{n+\gamma}$ in Eq. (48), for both second- and third-order accurate methods.

By subtracting Eqs. (51) and (49), we obtain

$$\int_t^{t+h} f dt\Big|_{\text{3 - point}} - \int_t^{t+h} f dt\Big|_{\text{4 - point}} = \frac{(1-2\gamma)h^4}{72} f^{(3)}(t) + O\left(h^5\right) \tag{53}$$

which shows the difference between the numerical impulses obtained by the three- and four-point Newton-Cotes formulas to be proportional to h^4 per step, h^3globally. Therefore, for the second-order accurate ρ_∞-Bathe method, using the load at the sub-step calculated from the Newton-Cotes formulas involving more than three points would provide marginal differences.

Likewise, calculating the sub-step load for the third-order accurate ρ_∞-Bathe method by using Newton-Cotes formulas involving more than four points would hardly increase the solution accuracy. We may check that the difference between the numerical impulse calculated from the four- and five-point Newton-Cotes formulas is proportional to h^4globally:

$$\int_t^{t+h} f dt\Big|_{\text{4 - point}} - \int_t^{t+h} f dt\Big|_{\text{5 - point}} = \frac{(5\gamma^2 - 10\gamma + 4)h^5}{720} f^{(4)}(t) + O\left(h^6\right) \tag{54}$$

4. Numerical examples

We give in this section some example solutions that illustrate our theoretical findings summarized in Table 1, to which we refer.

4.1. A damped single-degree-of-freedom system (SDOF)

We consider a damped SDOF system with mass $m = 1$, dampingc $= 2$, stiffness$k = 100$, external force $f = \sin(\omega t)$, and solve for the response during the time duration $10T_0$, where T_0 is the free-vibration period. To compare the accuracy, we use the error norms

$$e_0 = \left(\frac{\sum_{i=0}^{10T_0/\Delta t}\left(u(i) - \bar{u}(i)\right)^2}{\sum_{i=0}^{10T_0/\Delta t}\left(\bar{u}(i)\right)^2}\right)^{0.5};$$
$$e_1 = \left(\frac{\sum_{i=0}^{10T_0/\Delta t}\left(v(i) - \bar{v}(i)\right)^2}{\sum_{i=0}^{10T_0/\Delta t}\left(\bar{v}(i)\right)^2}\right)^{0.5};$$
$$e_2 = \left(\frac{\sum_{i=0}^{10T_0/\Delta t}\left(a(i) - \bar{a}(i)\right)^2}{\sum_{i=0}^{10T_0/\Delta t}\left(\bar{a}(i)\right)^2}\right)^{0.5} \tag{55}$$

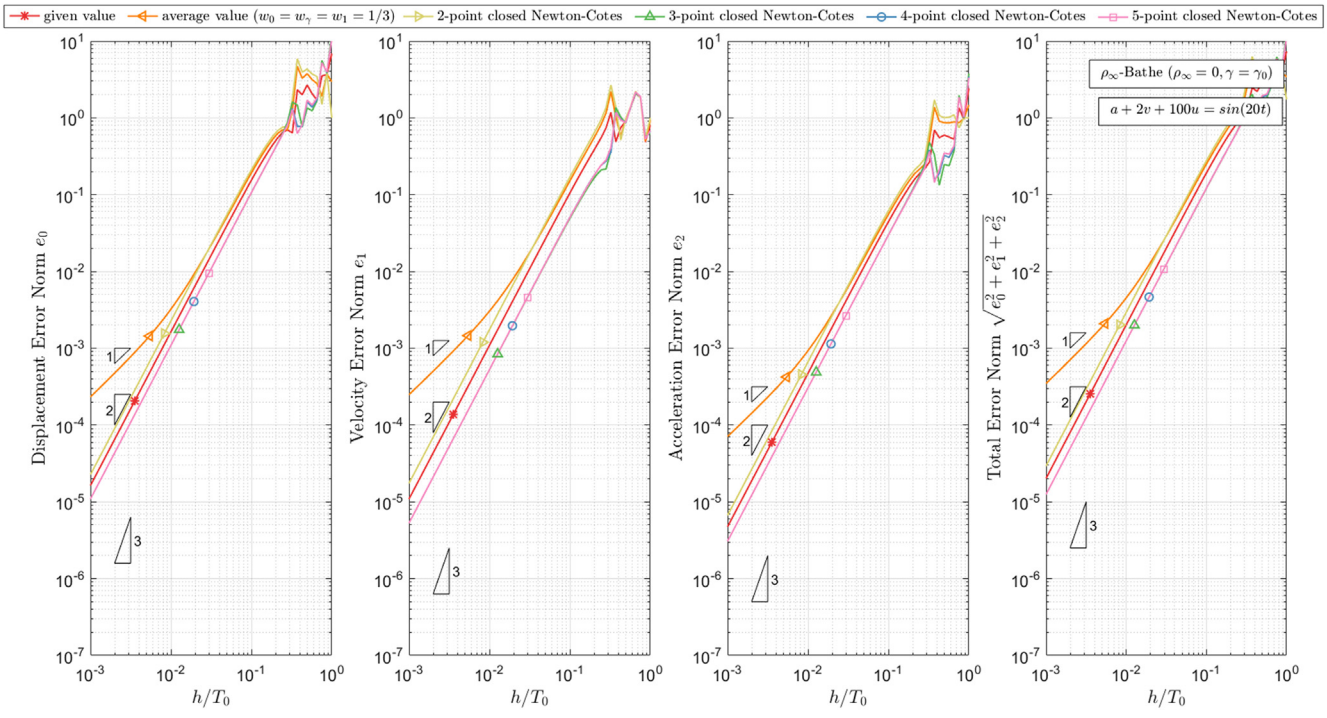

Fig. 1. Damped SDOF system solved by the ρ_∞-Bathe scheme for various values of $\hat{f}_{n+\gamma}$ when $\rho_\infty = 0$ with $\gamma = \gamma_0$.

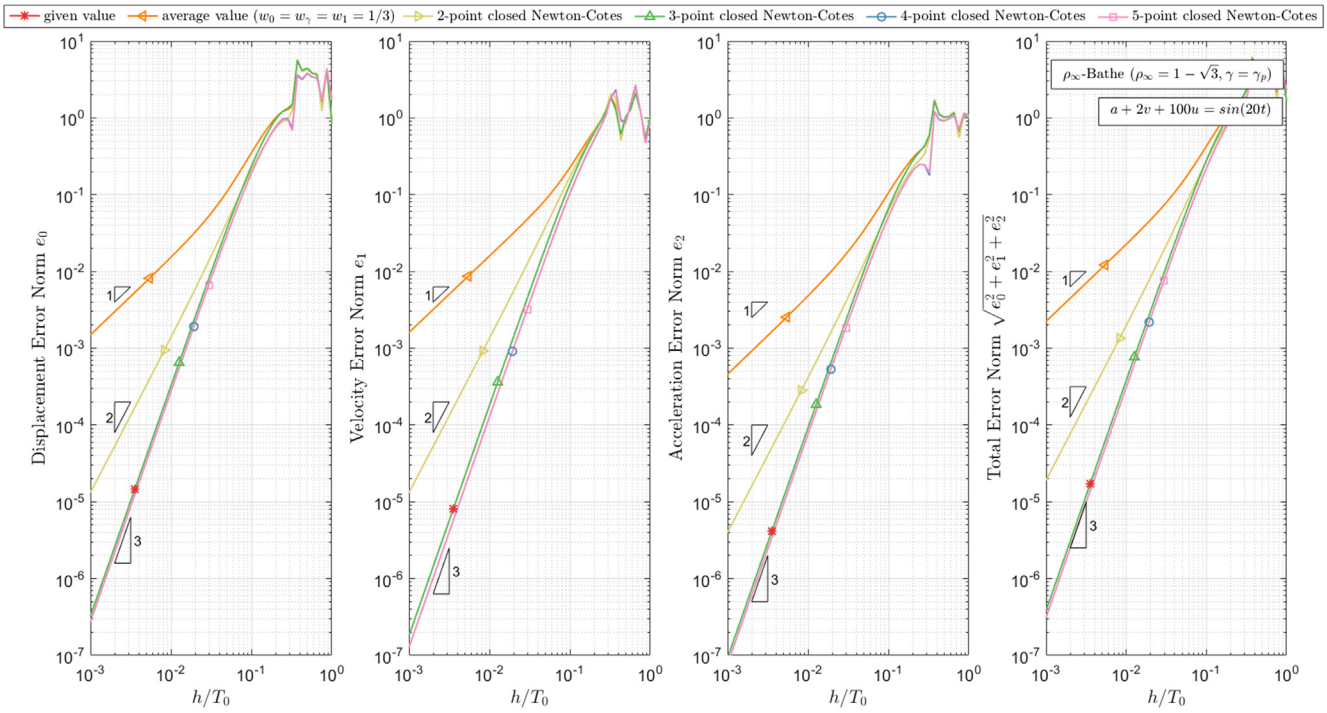

Fig. 2. Damped SDOF system solved by the ρ_∞-Bathe scheme for various values of $\hat{\boldsymbol{f}}_{n+\gamma}$ when $\rho_\infty = 1 - \sqrt{3}$ with $\gamma = \gamma_p$.

where u, v, a and $\bar{u}$, $\bar{v}$, $\bar{a}$ are the numerical and analytical (or reference) solutions, respectively.

Figs. 1-2 show the error norms of the displacement, velocity, acceleration, and its sum for the ρ_∞-Bathe schemes with $(\rho_\infty, \gamma) = (0, \gamma_0)$ and $(\rho_\infty, \gamma) = \left(1 - \sqrt{3}, \gamma_p\right)$, respectively. Since the actually given sub-step load provides second- and third-order accuracy for both the homogeneous and forced responses in the second- and third-order ρ_∞-Bathe schemes, respectively, the error norms have second- and third-order accuracy for $\rho_\infty = 0$ with $\gamma = \gamma_0$ and $\rho_\infty = 1 - \sqrt{3}$ with $\gamma = \gamma_p$, respectively.

The use of the average value and the value using the trapezoidal rule (two point Newton-Cotes) for the calculation of the sub-step

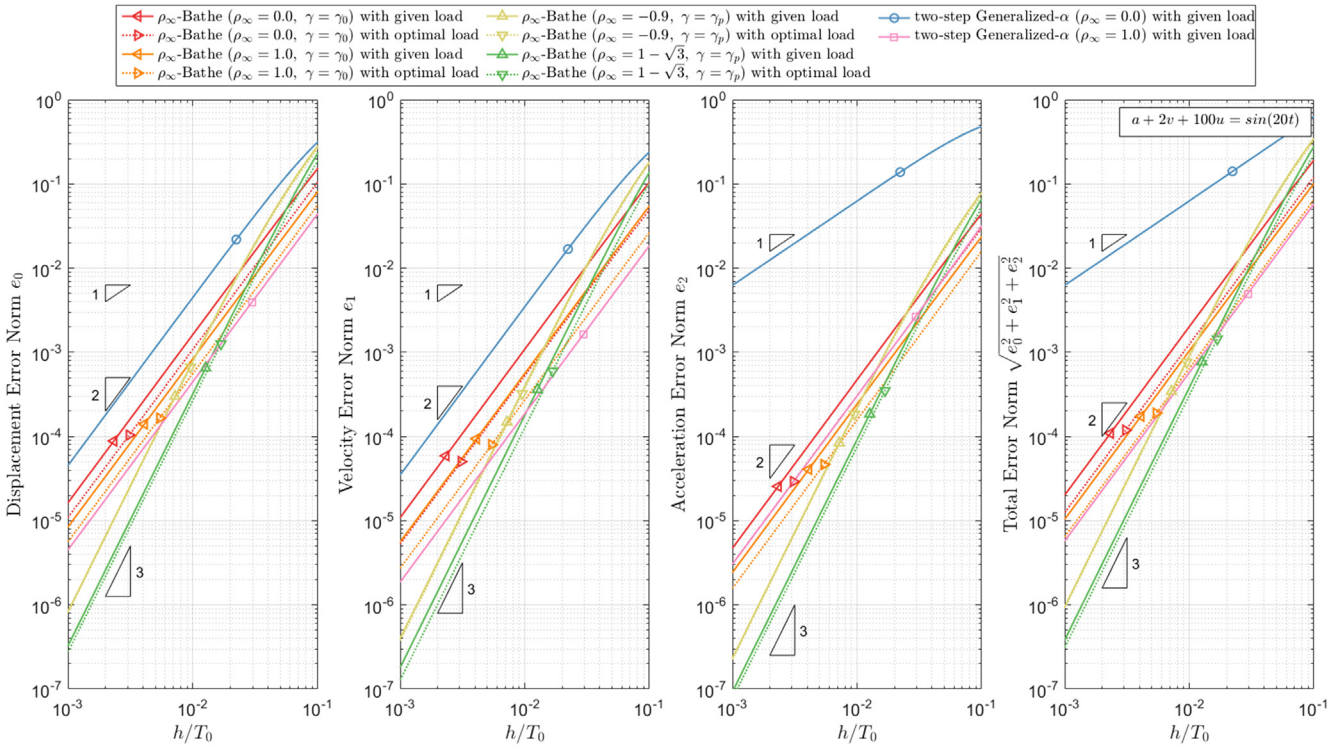

Fig. 3. Related error norms of the ρ_∞-Bathe scheme with given and optimal loads, and two-step generalized-α scheme with given loads.

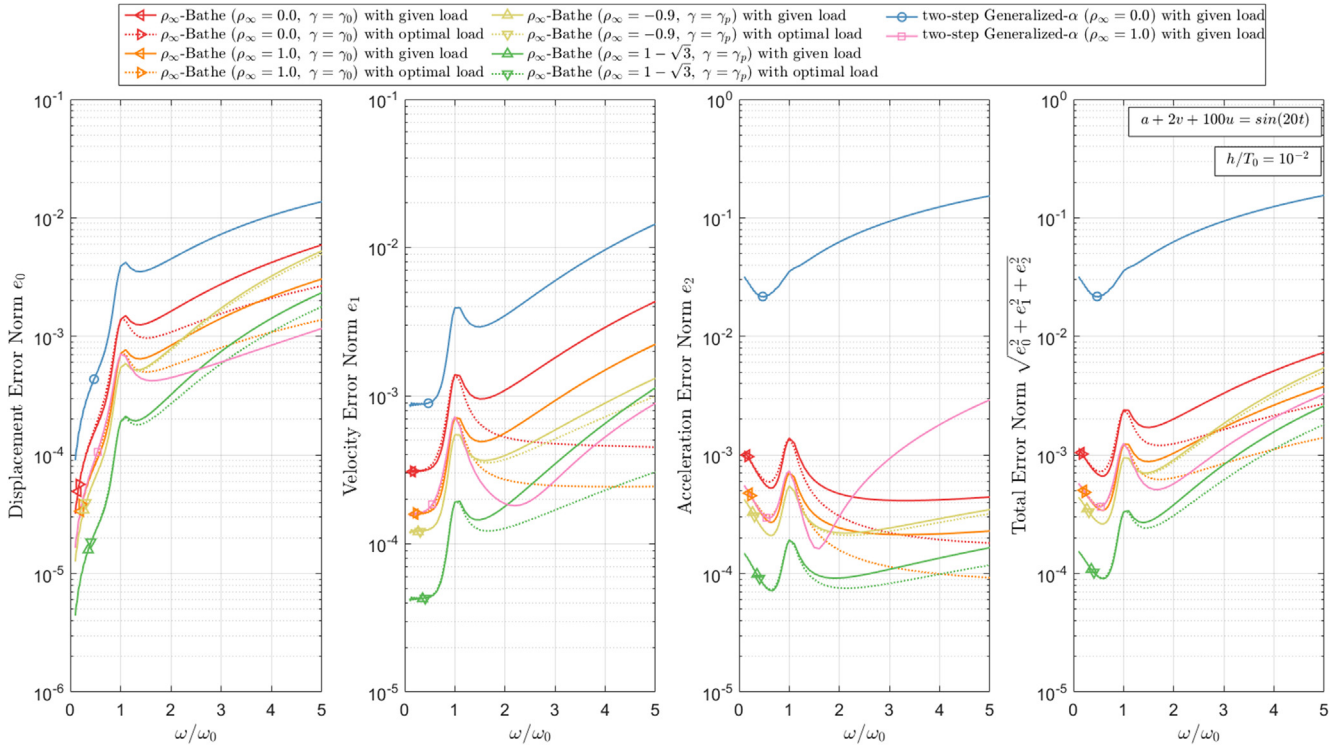

Fig. 4. Related error norms of the ρ_∞-Bathe scheme with given and optimal loads and two-step generalized-α scheme with given loads for various values of ω/ω_0 when $h/T_0 = 10^{-2}$.

load yields first- and second-order accurate solutions due to the first- and second-order accuracy in the calculation of the forced responses, respectively (See Eq. (24)).

Also, as we expected in Sections 3.2, for the case of second-order accuracy, $(\rho_\infty, \gamma) = (0, \gamma_0)$, the numerical errors using the three-, four-, and five-point Newton-Cotes formulas are almost the same. Likewise, for the ρ_∞-Bathe scheme with $(\rho_\infty, \gamma) = \left(1-\sqrt{3}, \gamma_p\right)$ having third-order accuracy, the sub-step loads evaluated from the four- and five-point Newton-Cotes formulas yield nearly the same solutions.

For the second- and third-order ρ_∞-Bathe schemes, the minimum response errors with the minimum number of weights are obtained when the three and four-point Newton-Cotes formulas are used. Therefore, in the remaining numerical tests, we refer to the sub-step loads modeled by three- and four-point Newton-Cotes formulas as the 'optimal load' for the second- and third-order ρ_∞-Bathe schemes, respectively.

Figs. 3–4 show the numerical errors for the ρ_∞-Bathe schemes with the various sub-step loads, and the two-step generalized-α schemes [8,9] with the given sub-step loads. In the two-step generalized-α scheme, we use the sub-step sizes $(h/2)$. As well known, the generalized-α method with $\rho_\infty \neq 1$ gives second-order accuracy for the displacement and velocity and first-order accuracy for the acceleration. In this example, the use of the ρ_∞-Bathe scheme with $\rho_\infty \in (-1, 1-\sqrt{3}]$ and $\gamma = \gamma_p$ yields smaller errors than all the considered second-order methods for sufficiently small time step sizes due to the third-order accuracy.

Notably, the optimal sub-step loads provide accuracy enhancements for all considered ρ_∞-Bathe methods. The amount of enhancement is more significant when the method has second-order accuracy. Fig. 4 shows the error norms for various values of ω/ω_0 when $h/T_0 = 10^{-2}$. For $\omega < \omega_0$, the optimal and given loads at the sub-step provide similar relative errors. On the other hand, the difference of numerical errors between the use of opti-

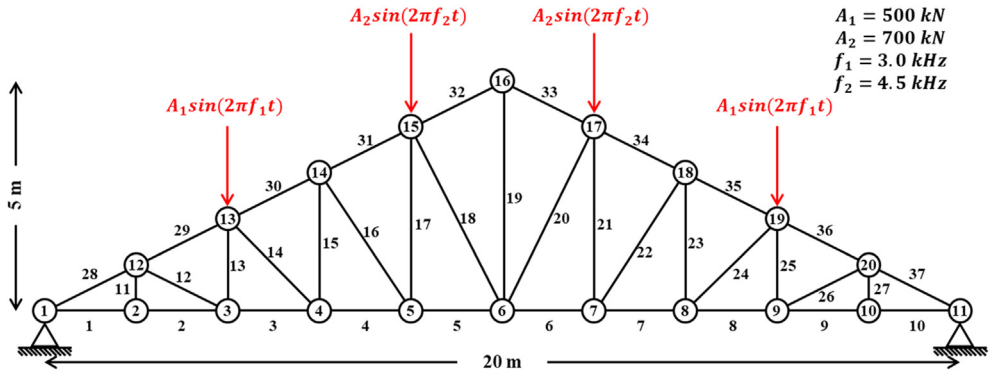

Fig. 5. A Howe truss under high frequency cyclic loads.

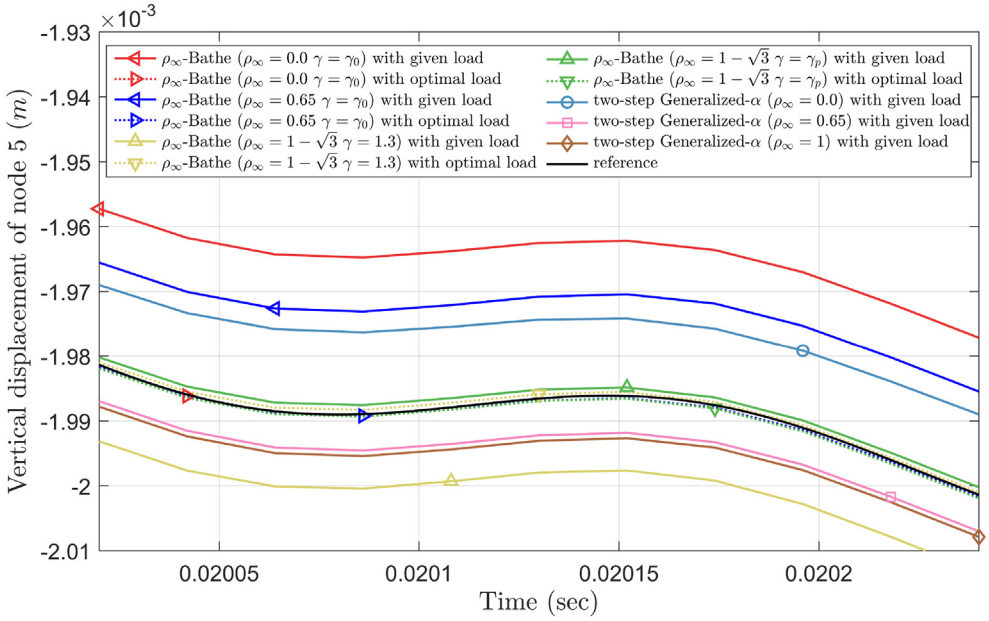

Fig. 6. Vertical displacement of node 5.

mal and given sub-step loads increases with an increase of ω when $\omega > \omega_0$.

4.2. A truss problem in two dimensions subjected to cyclic loading

We consider the truss shown in Fig. 5 subjected to four cyclic loads [15]. For all elements in the truss, we use the section area A = 3000 mm^2, density ρ = 8000 kg/m^3, and elastic modulus E = 4 GPa. The ρ_∞-Bathe schemes with the given and optimal sub-step loads, and the two-step generalized-α schemes with the given sub-step loads are compared. The time step size is $h = 2.2e-5$ sec(and $h/2$ for the generalized-α schemes). The reference solution is obtained with the ρ_∞-Bathe scheme ($\rho_\infty = 0$ and $\gamma = \gamma_0$), $h = 2.2\,e-6$ sec and the given sub-step loads used.

Figs. 6-8 show the vertical displacement of node 5, the horizontal displacement of node 13, and the relative errors of the system energies for the various time integration schemes. For the displacements, all solutions using the ρ_∞-Bathe schemes with the optimal loads provide accurate results. By looking at the system energies, we see that the use of the optimal loads reduces the relative errors by a factor of 10^2 compared to the use of the given loads.

4.3. A two-dimensional scalar wave propagation

We consider the solutions of the pre-stressed membrane problem [40,41,32] using the ρ_∞-Bathe schemes (Fig. 9). The governing equation for this 2D scalar wave propagation problem is

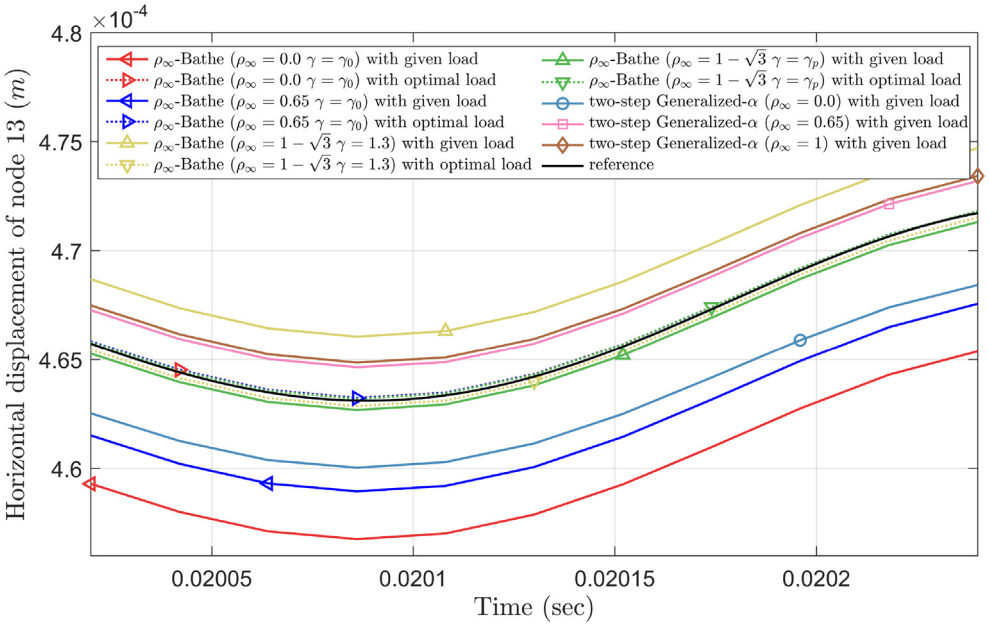

Fig. 7. Horizontal displacement of node 13.

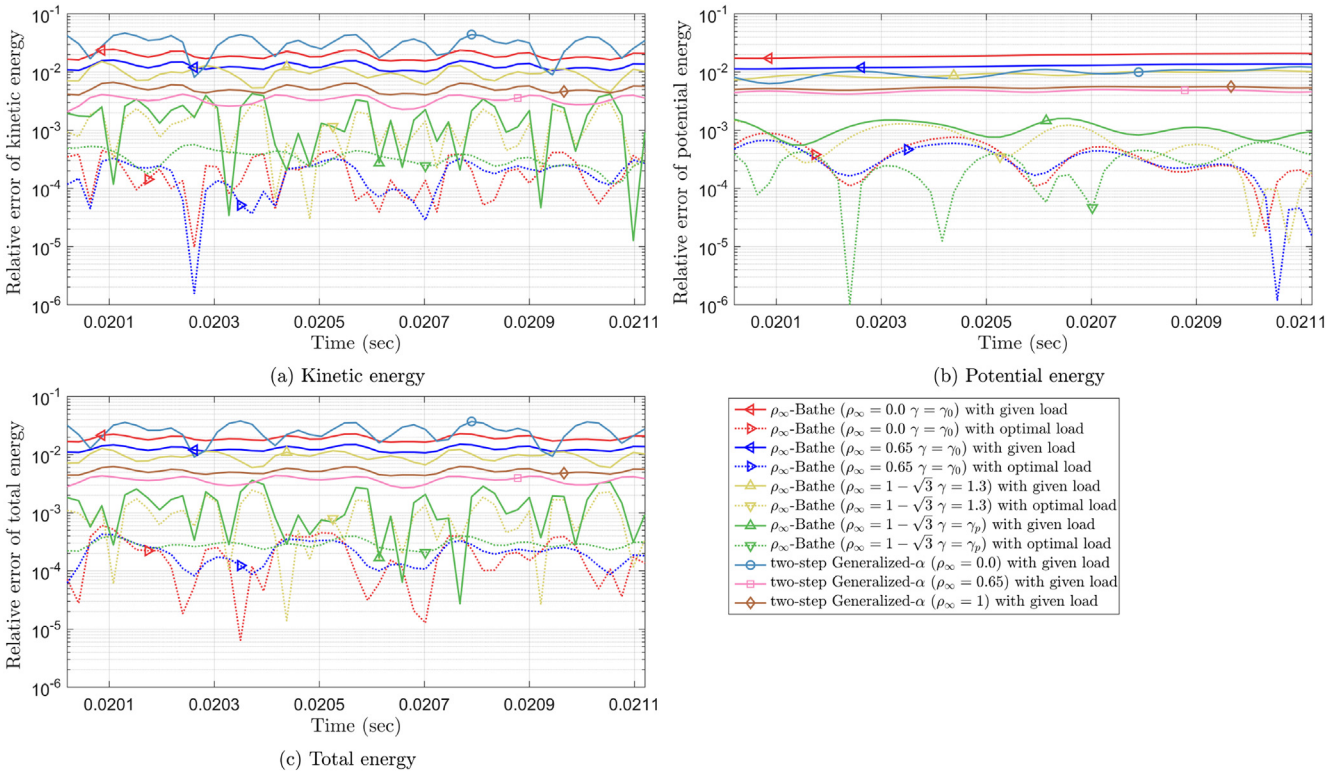

Fig. 8. Relative error of kinetic, potential, and total energies.

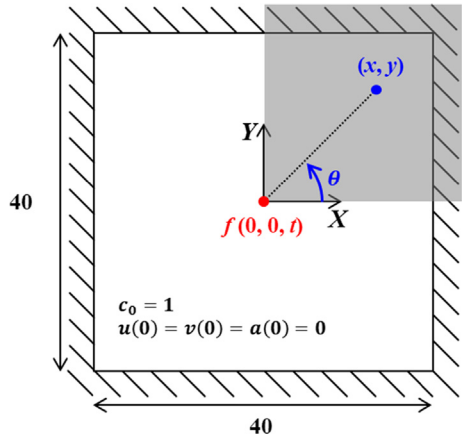

Fig. 9. 2D scalar wave propagation problem for a pre-stressed membrane, the shaded area is computational domain.

$$\frac{1}{c_0^2}\frac{\partial^2 u}{\partial t^2} = \frac{\partial^2 u}{\partial x^2} + \frac{\partial^2 u}{\partial y^2} + f(0, 0, t) \tag{56}$$

where u is the transverse displacement, and c_0 is exact wave speed, which is set to 1. We use the cyclic external load at the center of the membrane as

$$f(0, 0, t) = \sin(2\pi t)H(3 - t), \quad t > 0 \tag{57}$$

where H is the Heaviside step function. The exact solution of this problem is obtained using the Green's function $G(x, y, t)$[42]:

$$u(x, y, t) = \int_0^t f(\tau)G(x, y, t - \tau)d\tau \tag{58}$$

$$G(x, y, t) = \frac{H\left(c_0 t - \sqrt{x^2 + y^2}\right)}{2\pi c_0\sqrt{c_0^2 t^2 - x^2 - y^2}} \tag{59}$$

Due to symmetry, we only discretize the domain $[0, 20] \times [0, 20]$ using four-node elements. We determine the time step size, h by the CFL number $c_0 h/x_e$ where the side length of the elements is used as the characteristic length, x_e.

Figs. 10–11 show the numerical and analytical solutions of displacement and velocity variations for two propagation angles using the 120×120 and 280×280 element meshes. We see that the 120×120 mesh is not sufficiently fine to capture the wave shapes accurately when the ratio of the wavelength, λ, to the element size, x_e, is around 7. Using the mesh of 280×280 elements with the $\lambda/x_e \approx 17$, the second-order ρ_∞-Bathe scheme with the parameters $(\rho_\infty, \text{CFL}) = (0, 1)$ or $(0.65, 1.25)$ provides accurate solutions in both directions. In contrast, the third-order accurate methods with the considered values of parameters did not yield accurate solutions. As observed previously, a lower-order method might give more accuate solutions of wave propagation problems, see for example, Refs [28,29,32,16]

To solve a problem with an applied load of period T, we often use $h \leqslant T/10$ or equivalently $\omega \leqslant 2\pi/10h$. Also, to minimize the dispersion errors, we determine the time step size, h, by the CFL number and use $\text{CFL} \leq 1$, hence $h \approx 2/\omega_0$ for the linear finite elements. Therefore, in usual wave propagation analysis by direct time integrations with the linear finite element, we have $\omega/\omega_0 < 1$. Note that as shown in Fig. 4, when $\omega/\omega_0 < 1$, the given and the selected load at the sub-step provide nearly identical results for both the second- and third-order accurate ρ_∞-Bathe methods.

Fig. 12 shows the relative error norms of displacements and velocities calculated by the ρ_∞-Bathe schemes with the given loads and the optimal loads. As expected, we observe that the given and optimal loads provide practically the same results.

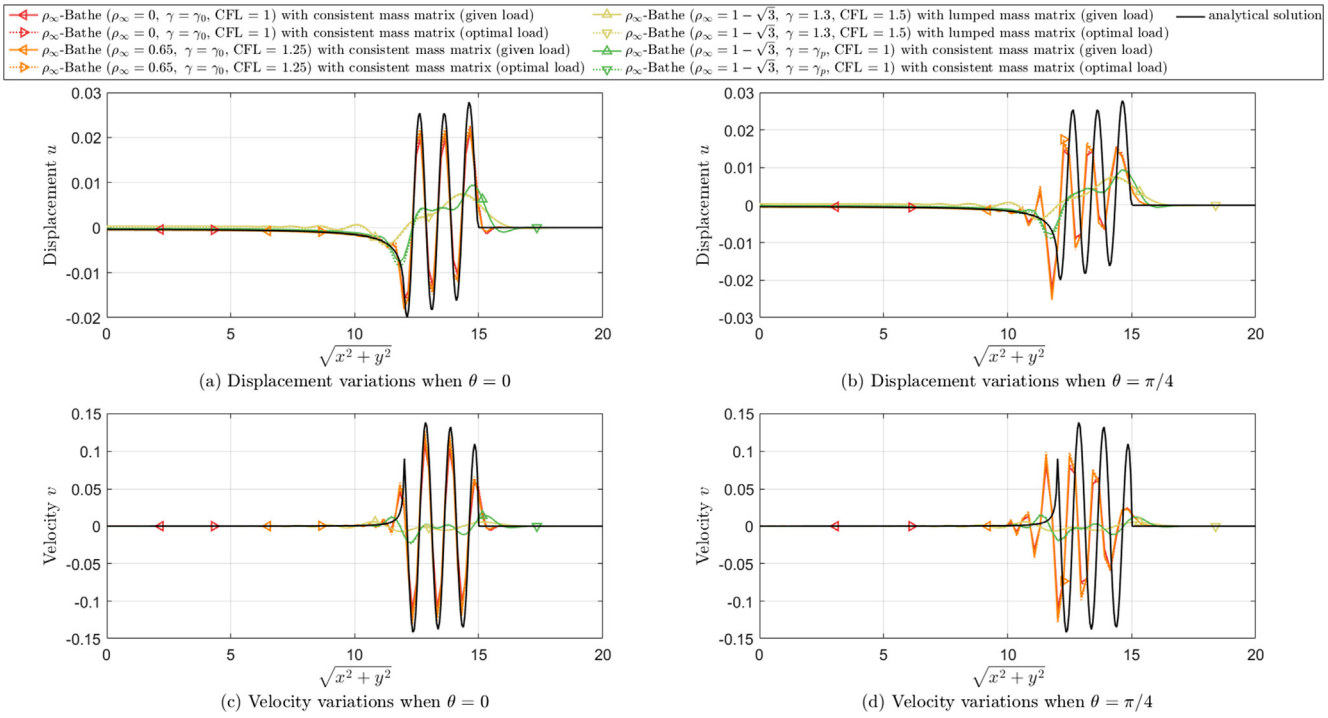

(a) Displacement variations when $\theta = 0$

(b) Displacement variations when $\theta = \pi/4$

(c) Velocity variations when $\theta = 0$

(d) Velocity variations when $\theta = \pi/4$

Fig. 10. Transverse displacement and velocity variations for two propagation angles at time $t = 15$ with 120 by 120 finite element mesh.

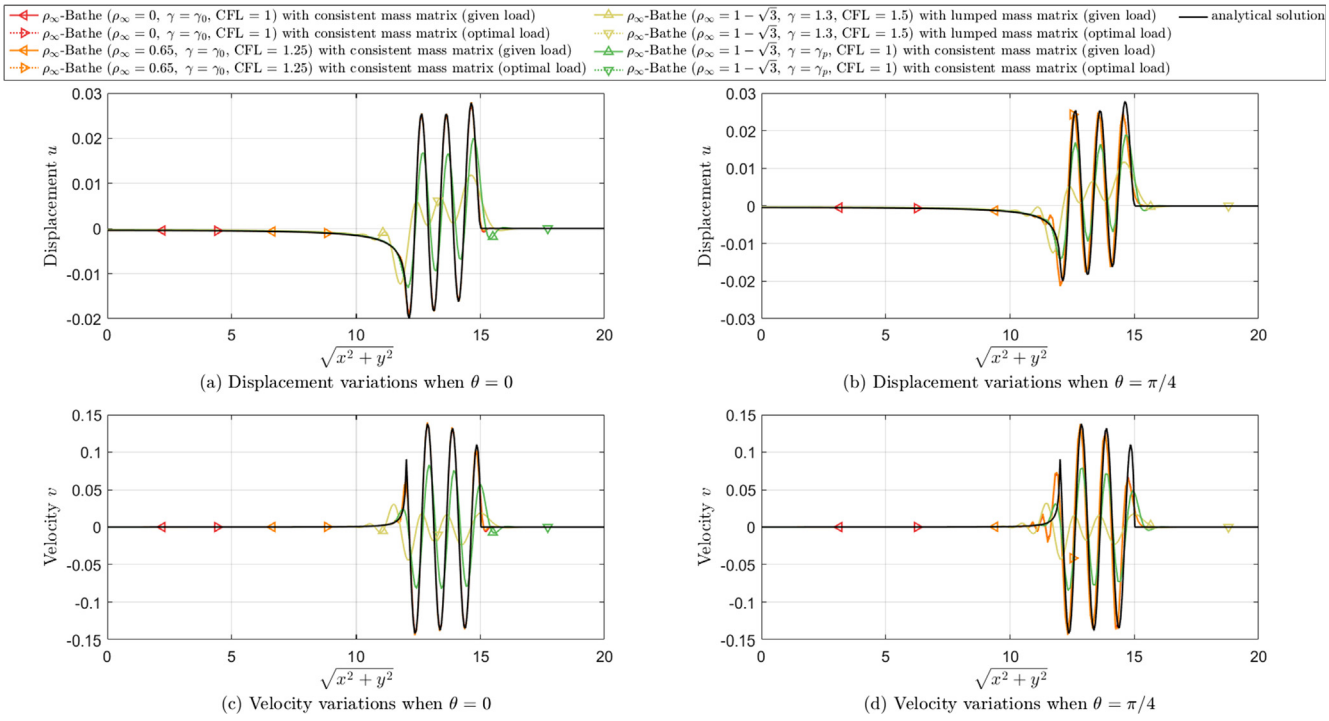

(a) Displacement variations when $\theta = 0$

(b) Displacement variations when $\theta = \pi/4$

(c) Velocity variations when $\theta = 0$

(d) Velocity variations when $\theta = \pi/4$

Fig. 11. Transverse displacement and velocity variations for two propagation angles at time $t = 15$ with 280 by 280 finite element mesh.

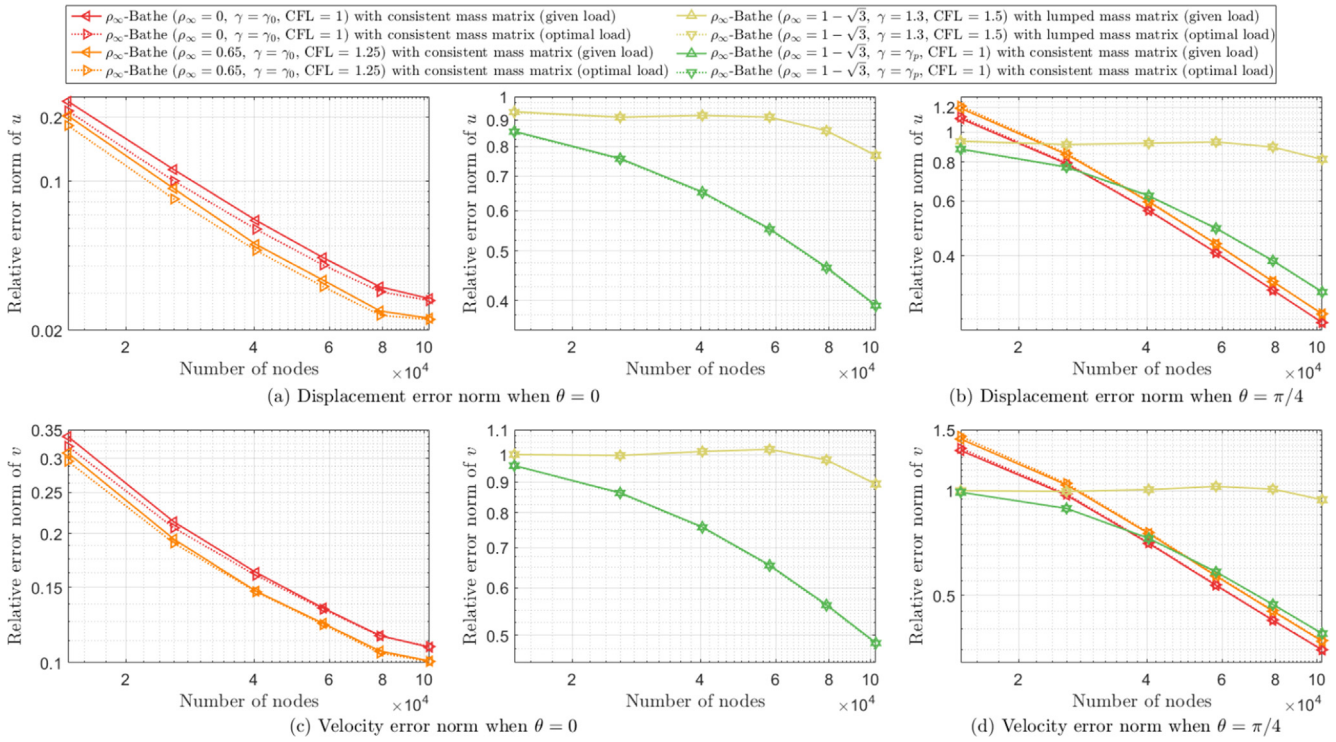

Fig. 12. Relative error norms of the displacement and velocity variations for two propagation angles at time $t = 15$.

5. Concluding remarks

In this paper, we considered the load used at the sub-step of the ρ_∞-Bathe method to enhance the solution accuracy in forced responses. We first analysed the local and global truncation errors by using the two-level form of the scheme. We focused on selecting (or "modelling") the sub-step loads in the form of a weighted linear sum of the given external loads at various time points, and found the optimal weights on the loading to minimize the leading terms of the global truncation errors in forced responses.

We then performed a numerical impulse analysis and obtained appropriate weights for the sub-step loading. The results from the numerical impulse solution are found to be the same as when using the two-, three-, four-, and five-point Newton-Cotes formulas. As these formulas are also arrived at by minimizing the truncation error, we identified that the use of the three- and four-point Newton-Cotes rules for selecting the sub-step load are optimal, respectively for the second- and third-order accuracy ρ_∞-Bathe schemes.

In summary, when the external loads are only available at the full step, we use the load approximated by the trapezoidal rule in Eq. (48). Otherwise, for the second- and third-order accurate ρ_∞-Bathe method (that is, with γ_0 in Eq. (26), and with γ_p in Eq. (28), respectively), the loads in Eq. (50) and (52) are recommended, respectively. When $\omega/\omega_0 > 1$, where ω is the frequency of the applied load and ω_0 is the natural frequency of the system analysed, which is not usually the case in a wave propagation analysis but often encountered in structural analyses, we may obtain enhanced solution accuracy by use of the selected sub-step loads for both the second- and third-order accurate Bathe methods.

Even though the solution accuracy may not necessarily increase significantly for a practical analysis, the study is nevertheless important, because the idea of increasing the accuracy by a judicious load selection at the sub-step in the ρ_∞-Bathe method is very valuable to explore, as we did in this paper.

Note that while we evaluated the external loads at the sub-step to enhance the solution accuracy of a forced response, the time integration method itself has not been changed; therefore, all beneficial characteristics of the ρ_∞-Bathe scheme are maintained, and almost no additional computational cost is needed.

A valuable future endeavor is to identify an even better use of the values of parameters or to modify the procedures required in the 'internal' calculations corresponding to the sub-step for further enhancement of the solution accuracy. Also, the presented framework to identify the optimal load at a sub-step should be valuable for use with other existing or future methods adopting a composite time stepping strategy.

Declaration of Competing Interest

The authors declare that they have no known competing financial interests or personal relationships that could have appeared to influence the work reported in this paper.

Acknowledgment

This work was partly supported by the Young Scientist Grants-Outstanding Track (Grant No. NRF-2021R1C1C1011494) through the National Research Foundation of Korea (NRF) funded by the Ministry of Science and ICT.

Appendix. The amplification matrix A and the direct load vector B

For the ρ_∞-Bathe scheme, the amplification matrix and direct load vector of the two-level form are as follows:

$$\boldsymbol{A} = \frac{1}{D_1 D_2}\begin{pmatrix} a_{11} & a_{12} \\ a_{21} & a_{22} \end{pmatrix}, \quad \boldsymbol{B} = \frac{1}{D_1 D_2}\begin{pmatrix} b_1 \\ b_2 \end{pmatrix}$$

where

$$
\begin{aligned}
a_{11} &= (q_1^2\gamma^2 - 2q_1^2\gamma + q_1 - 0.25)\gamma^2\Omega_0^4 + (4q_1^2\gamma^2 - 2q_1\gamma^2 + \gamma - 1)\gamma\Omega_0^3\zeta \\
&\quad + (4q_1^2\gamma^2 + \gamma^2 - 4q_1\gamma - 1 + 4(1 - 2q_1\gamma)\gamma\zeta^2)\Omega_0^2 + 4(1 - 2q_1\gamma + \gamma)\Omega_0\zeta + 4 \\
a_{12} &= h\Big((4q_1^2\gamma - 2q_1\gamma + \gamma - 2q_1)\gamma\Omega_0^2 + 4(1 - 2q_1)\gamma\Omega_0\zeta + 4\Big) \\
a_{21} &= -\tfrac{\Omega_0^2}{h}\Big((4q_1^2\gamma - 2q_1\gamma + \gamma - 2q_1)\gamma\Omega_0^2 + 4(1 - 2q_1)\gamma\Omega_0\zeta + 4\Big) \\
a_{22} &= (q_1^2\gamma^2 - 2q_1^2\gamma + q_1 - 0.25)\gamma^2\Omega_0^4 + (4q_1^2\gamma^2 - 2q_1\gamma^2 - 8q_1^2\gamma + 4q_1\gamma - \gamma + 4q_1 - 1)\gamma\Omega_0^3\zeta \\
&\quad + (4q_1^2\gamma^2 + \gamma^2 - 4q_1\gamma - 1 + 4(-2q_1\gamma + 4q_1 - 1)\gamma\zeta^2)\Omega_0^2 + 4(-2q_1\gamma + \gamma - 1)\Omega_0\zeta + 4
\end{aligned}
$$

$$
b_1 = \tfrac{h^2}{4}\begin{pmatrix}
(4(f_{n+1} - f_n)q_1^2\gamma^4 + 4(2f_nq_1 - f_{n+1})q_1\gamma^3 + (f_n + f_{n+1} - 4q_1f_n)\gamma^2)\Omega_0^2 \\
+4\begin{pmatrix} 4(f_{n+1} - f_n)q_1^2\gamma^3 + 4\Big(\Big(f_n - \hat{f}_{n+\gamma}\Big)q_1 - f_{n+1}\Big)q_1\gamma^2 \\ +\Big((f_n + f_{n+1}) + 2\Big(\hat{f}_{n+\gamma} - f_n\Big)q_1\Big)\gamma \end{pmatrix}\Omega_0\zeta \\
-16(f_n - f_{n+1})q_1^2\gamma^2 + 8\Big(2\Big(f_n - \hat{f}_{n+\gamma}\Big)q_1 + f_n - 2f_{n+1} + \hat{f}_{n+\gamma}\Big)q_1\gamma \\
+4(f_n + f_{n+1}) - 8q_1\Big(f_n + \hat{f}_{n+\gamma}\Big)
\end{pmatrix}
$$

$$
b_2 = \tfrac{h}{2}\begin{pmatrix}
\Big(2(f_n - 2f_{n+1})q_1\gamma^3 + \Big((f_n + f_{n+1}) - 4f_nq_1 + 4\Big(f_n + \hat{f}_{n+\gamma}\Big)q_1^2\Big)\gamma^2 - 2\Big(f_n + \hat{f}_{n+\gamma}\Big)q_1\gamma\Big)\Omega_0^2 \\
+(8(f_n - f_{n+1})q_1\gamma^2 - 16f_nq_1\gamma + 4(f_n + f_{n+1}))\Omega_0\zeta \\
+8(f_n - f_{n+1})q_1\gamma + 4(f_n + f_{n+1}) - 8\Big(f_n - \hat{f}_{n+\gamma}\Big)q_1
\end{pmatrix}
$$

with $D_1 = \gamma^2\Omega_0^2 + 4\gamma\Omega_0\zeta + 4$ and $D_2 = (0.5 - \gamma q_1)^2\Omega_0^2 + (1 - 2\gamma q_1)\Omega_0\zeta + 1$, and $\Omega_0 = \omega_0 h$.

References

[1] Bathe KJ. In: The finite element method, encyclopedia of computer science and engineering. Hoboken, New Jersey, J: Wiley and Sons; 2009. p. 1253–64.
[2] Bathe KJ. Frontiers in finite element procedures & applications, chapter 1 in computational methods for engineering technology. Stirlingshire, Scotland: Saxe-Coburg Publications; 2014.
[3] Bathe KJ. Finite element procedures, 2nd ed. In: Bathe KJ, editor. Watertown, MA; also published by Higher Education Press China; 2016.
[4] Newmark NM. A method of computation for structural dynamics. J Eng Mech Div (ASCE) 1959;85:67–94.
[5] Bathe KJ, Wilson EL. Stability and accuracy analysis of direct integration methods. Int J Earthquake Eng Struct Dyn 1973;1:283–91.
[6] Hilber HM, Hughes TJR, Taylor RL. Improved numerical dissipation for time integration algorithms in structural dynamics. Earthquake Eng Struct Dyn 1977;5:283–92.
[7] Wood WL, Bossak M, Zienkiewicz OC. An alpha modification of Newmark's method. Int J Numer Meth Eng 1980;15:1562–6.
[8] Shao HP, Cai CW. The direct integration three-parameters optimal schemes for structural dynamics. In: Proceedings of the international conference: machine dynamics and engineering applications. Xi'an Jiaotong University Press, C16–20; 1988.
[9] Chung J, Hulbert GM. A time integration algorithm for structural dynamics with improved numerical dissipation: the generalized-alpha method. J Appl Mech (ASME) 1993;60:371–5.
[10] Tamma KK, Zhou X, Sha D. The time dimension: a theory towards the evolution, classification, characterization and design of computational algorithms for transient/dynamic applications. Arch Comput Methods Eng 2000;7:67–290.
[11] Zhou X, Tamma KK. Design, analysis, and synthesis of generalized single step single solve and optimal algorithms for structural dynamics. Int J Numer Meth Eng 2004;59:597–668.
[12] Chang SY. Dissipative, noniterative integration algorithms with unconditional stability for mildly nonlinear structural dynamic problems. Nonlinear Dyn 2015;79(2):1625–49.
[13] Dong S. BDF-like methods for nonlinear dynamic analysis. J Comput Phys 2010;229(8):3019–45.
[14] Chandra Y, Zhou Y, Stanciulescu I, Eason T, Spottswood S. A robust composite time integration scheme for snap-through problems. Comput Mech 2015;55 (5):1041–56.
[15] Wen WB, Wei K, Lei HS, Duan SY, Fang DN. A novel sub-step composite implicit time integration scheme for structural dynamics. Comput Struct 2017;182:176–86.
[16] Huang C, Fu M. A composite collocation method with low-period elongation for structural dynamics problems. Comput Struct 2018;195:74–84.
[17] Kim W, Choi SY. An improved implicit time integration algorithm: the generalized composite time integration algorithm. Comput Struct 2018;196:341–54.
[18] Zhang HM, Xing YF. Optimization of a class of composite method for structural dynamics. Comput Struct 2018;202:60–73.
[19] Li J, Yu K. An alternative to the Bathe algorithm. Appl Math Model 2019;69:255–72.
[20] Xing Y, Ji Y. On the construction of a type of composite time integration methods. Comput Struct 2019;221:157–78.
[21] Zhang J. A-stable two-step time integration methods with controllable numerical dissipation for structural dynamics. Int J Numer Meth Eng 2020;121(1):54–92.
[22] Ji Y, Xing Y. An optimized three-sub-step composite time integration method with controllable numerical dissipation. Comput Struct 2020;106210.
[23] Li J, Yu K. A novel family of composite sub-step algorithms with desired numerical dissipations for structural dynamics. Arch Appl Mech 2020;90:737–72.
[24] Zhang H, Zhang R, Xing Y, Masarati P. On the optimization of n-sub-step composite time integration methods. Nonlinear Dyn 2020;1–24.
[25] Wen W, Deng S, Wang N, Duan S, Fang D. An improved sub-step time-marching procedure for linear and nonlinear dynamics with high-order accuracy and high-efficient energy conservation. Appl Math Model 2021;90:78–100.
[26] Bathe KJ, Baig MMI. On a composite implicit time integration procedure for nonlinear dynamics. Comput Struct 2005;83:2513–4.
[27] Bathe KJ. Conserving energy and momentum in nonlinear dynamics: a simple implicit time integration scheme. Comput Struct 2007;85:437–45.
[28] Malakiyeh MM, Shojaee S, Bathe KJ. The Bathe time integration method revisited for prescribing desired numerical dissipation. Comput Struct 2019;212:289–98.
[29] Malakiyeh MM, Shojaee S, Hamzehei-Javaran S, Bathe KJ. New insight into the β_1/β_2-Bathe time integration scheme when L-stable. Comput Struct 2021;245:106433.
[30] Noh G, Bathe KJ. The Bathe time integration method with controllable spectral radius: The ρ_∞-Bathe method. Comput Struct 2019;212:299–310.
[31] Noh G, Bathe KJ. For direct time integrations: a comparison of the Newmark and ρ_∞-Bathe schemes. Comput Struct 2019;225:1–12.
[32] Kwon S-B, Bathe KJ, Noh G. An analysis of implicit time integration schemes for wave propagations. Comput Struct 2020;230:106188.
[33] Bathe KJ, Noh G. Insight into an implicit time integration scheme for structural dynamics. Comput Struct 2012;98–99:1–6.
[34] Noh G, Bathe KJ. Further insights into an implicit time integration scheme for structural dynamics. Comput Struct 2018;202:15–24.
[35] Chen CC, Robinson AR. Improved time-history analysis for structural dynamics. I: Treatment of rapid variation of excitation and material nonlinearity. J Eng Mech 1993;119:2496–513.

[36] Chang S-Y. Analytical study of the superiority of momentum equations of motion for impulsive loads. Comput Struct 2001;79:1377–94.
[37] Chang S-Y. A technique for overcoming load discontinuity in using Newmark method. J Sound Vib 2007;304:556–69.
[38] Chang S-Y. Approach for overcoming numerical inaccuracy caused by load discontinuity. J Eng Mech 2007;133:555–65.
[39] Chang S-Y. Remedy for load discontinuity in time history analysis. Int. J. Struct. Stab. Dy. 2012;12:337–58.
[40] Noh G, Ham S, Bathe KJ. Performance of an implicit time integration scheme in the analysis of wave propagations. Comput Struct 2013;123:93–105.
[41] Noh G, Bathe KJ. An explicit time integration scheme for the analysis of wave propagations. Comput Struct 2013;129:178–93.
[42] Kwon S-B, Lee J-M. A non-oscillatory time integration method for numerical simulation of stress wave propagations. Comput Struct 2017;192:248–68.
[43] Alexandre D, Emmanuel D Vincent. Accuracy of one-step integration schemes for damped/forced linear structural dynamics. Int J Numer Meth Engng 2014;99:333–53.
[44] Choi B, Bathe KJ, Noh G, Time splitting ratio of an implicit time integration scheme for higher-order accuracy in structural dynamics and heat equations (in preparation).
[45] Sun Y, Luo L, Chen K, Qin X, Zhang Q. A time-domain method for load identification using moving weighted least square technique. Comput Struct 2020;234:106254.